

Article

Synthesis of Micro-Spikes and Herringbones Structures by Femtosecond Laser Pulses on a Titanium Plate—A New Material for Water Organic Pollutants Degradation

Joanna Kisała ^{1,*},† , Iaroslav Gnilitskyi ^{2,3,†} , Bogumił Cieniek ¹ , Piotr Krzemiński ⁴, Michał Marchewka ⁴ , Adriana Barylyak ⁵ and Yaroslav Bobitski ^{2,4,*} 

¹ College of Natural Sciences, University of Rzeszow, Pigionia 1, 35-959 Rzeszow, Poland; bcieniek@ur.edu.pl

² Department of Photonics, Lviv Polytechnic National University, 1 Sviatoho Yura Sq., 79013 Lviv, Ukraine; iaroslav.gnilitskyi@novinano.com

³ NoviNano Lab LLC, Paternaka Str. 5, 79000 Lviv, Ukraine

⁴ Center for Microelectronics and Nanotechnology, Institute of Physics, University of Rzeszow, Pigionia 1, 35-959 Rzeszow, Poland; pkrzeminski@ur.edu.pl (P.K.); mmarchewka@ur.edu.pl (M.M.)

⁵ Department of Therapeutic Dentistry, Danylo Halitsky Lviv National Medicinal University, Pekarska Str. 69, 79010 Lviv, Ukraine; adriana.barylyak5@gmail.com

* Correspondence: jkisała@ur.edu.pl (J.K.); yaroslav.v.bobytskyi@lpnu.ua (Y.B.)

† These authors contributed equally.



Citation: Kisała, J.; Gnilitskyi, I.; Cieniek, B.; Krzemiński, P.; Marchewka, M.; Barylyak, A.; Bobitski, Y. Synthesis of Micro-Spikes and Herringbones Structures by Femtosecond Laser Pulses on a Titanium Plate—A New Material for Water Organic Pollutants Degradation. *Materials* **2021**, *14*, 5556. <https://doi.org/10.3390/ma14195556>

Academic Editors: Emmanuel Unuabonah and Andreas Taubert

Received: 15 August 2021

Accepted: 19 September 2021

Published: 24 September 2021

Publisher's Note: MDPI stays neutral with regard to jurisdictional claims in published maps and institutional affiliations.



Copyright: © 2021 by the authors. Licensee MDPI, Basel, Switzerland. This article is an open access article distributed under the terms and conditions of the Creative Commons Attribution (CC BY) license (<https://creativecommons.org/licenses/by/4.0/>).

Abstract: (1) Background: The shrinkage of water resources, as well as the deterioration of its quality as a result of industrial human activities, requires a comprehensive approach relative to its protection. Advanced oxidation processes show high potential for the degradation of organic pollutants in water and wastewater. TiO₂ is the most popular photocatalyst because of its oxidizing ability, chemical stability and low cost. The major drawback of using it in powdered form is the difficulty of separation from the reaction mixture. The solution to this problem may be immobilization on a support (glass beads, molecular sieves, etc.). In order to avoid these difficulties, the authors propose to prepare a catalyst as a titanium plate covered with an oxide layer obtained with laser treatment. (2) Methods: In the present work, we generated titanium oxide structures using a cheap and fast method based on femtosecond laser pulses. The structured plates were tested in the reaction of methylene blue (MB) degradation under UVA irradiation (365 nm). The photocatalytic activity and kinetic properties for the degradation of MB are provided. (3) Results: Studies of X-ray diffraction (XRD) and scanning electron microscopy (SEM) confirm a titanium oxide layer with laser-induced generated structures that are called “spikes” and “herringbones”. The structured plates were effective photocatalysts, and their activity depends on the structure of the oxide layer (spike and herringbone). (4) Conclusions: The immobilization of the catalyst on a solid support can be performed in a fast and reproducible manner by using the technique of laser ablation. The layers obtained with this method have been shown to have catalytic properties.

Keywords: femtosecond laser processing self-organized microstructures; herringbone structure; engineered materials; photocatalysis; waste water treatment

1. Introduction

In recent years, there has been great concern over many serious environmental problems. The most important is the safety of water. There is a wide range of chemical and biological contaminants that may be found in water. The need for clean water places increased stress on the removal of organic pollutants and toxic heavy metal ions from water sources. There are several processes performed in order to improve water quality, such as chemical, physical, physico-chemical and biological processes. Chemical treatment includes precipitation, chemical disinfection, oxidation, advanced oxidation processes, and ion exchange [1].

Advanced oxidation technologies are based on in situ generation of strong oxidants, i.e., hydroxyl radicals, for the oxidation of organic pollutants. AOPs use strong oxidizing agents, such as hydrogen peroxide (H₂O₂) or ozone (O₃), catalysts (iron ions, electrodes and metal oxides) and irradiation (UV light, visible-light and ultrasounds), separately or in combination under mild conditions (low temperature and pressure) [2]. Among different available AOPs, those driven by light seem to be attractive because of the abundance of solar light in regions where water scarcity is high and due to their relatively low costs and high efficiencies.

Titanium (IV) oxide (TiO₂) is commonly known as a photocatalyst for the photodegradation of organic pollutants [3]. By using heterogeneous catalysts in wastewater treatment, two key problems are encountered: (i) the efficiency of the catalytic reaction and (ii) recovering photocatalyst after treatment. TiO₂ is usually applied in suspension mode, resulting in a high surface-area-to-volume ratio. However, recovering this TiO₂ powder slurry from treated wastewater requires filtration. Isolation of TiO₂ slurry may clog the filter membrane, and catalyst particles will eventually pass through the porous filter, rendering the recovery process less efficient. The solution to this problem may be the immobilization of powder on a support (glass beads, molecular sieves, etc.). Hence, the use of a bulk-supporting substrate with a directly grown oxide layer is a reasonable choice to eliminate powder drawbacks.

The appearance of non-thermal ablation mechanisms much advanced surface modifications by femtosecond lasers [4]. It rendered these lasers attractive for surface treatments, which are aimed at the absence of heat-induced material damage on semiconductors, dielectric and metallic materials [5]. Apart from laser ablation, linearly polarized femtosecond laser pulses enable the formation of self-organised nanostructures, which are so-called laser-induced periodic surface structures, i.e., LIPSS [6]. LIPSS, otherwise known as surface ripples or nano gratings, are parallel periodic grooves produced on the surface of materials by laser irradiation, having a period proportional to the laser's wavelength. Such sub-microstructures and nanostructures have a huge potential of application in such fields as tribology [7,8] and wettability [9–13] given their ability to improve the adhesion strength [13], as well as by improving differentiation of tissue cells [13–15], and surface colorization [10].

Aside from LIPSS, the femtosecond lasers allow the formation of the various types of nano/microstructures by tuning their parameters. For example, hexagons [16], grooves [6] and spikes [17] were formed by using of various number of laser pulses and tuning laser fluence. By changing the angle of incidence for laser light or a laser wavelength, the period of structures can be determined. Moreover, by varying laser fluence, the height and morphology can be changed, whereas the structure direction may be tuned by optics configuration. To summarize, the femtosecond nano- or microstructuring is a one-step process, which does not require vacuum or other arrangements and which proves the flexibility and applicability relative to original materials for various purposes. During femtosecond laser processing and formation on the surface, self-organized structures form an oxidative layer. The formation of TiO₂ and ZrO while LIPSS creation occurrence was observed in [18].

Tsukamoto et al. [19] reported the formation of cone-like microstructures on a titanium (Ti) plate by femtosecond laser ablation. Wavelength, pulse length and repetition rates were 800 nm, 100 fs and 1 kHz, respectively. The number of laser pulses varied from 10 to 230. The experiment was performed under vacuum. The period of the periodic nanostructures was about 700 nm. The spike structures were also obtained by Heitz et al. [20] in their experiments, where Ti-alloy substrates were irradiated in the air by Ti:sapphire femtosecond laser pulses (790 nm, 30 fs and 1 kHz). The spike structures were covered by more regular parallel submicrometric LIPSS grating structures, resulting in a hierarchical surface morphology. The periodicity of the LIPSS grating is about 300–350 nm. Liang et al. [21] fabricated a hierarchical TiO_{2-x} photoelectrode directly in situ on a metal substrate through femtosecond laser processing and anodization. Laser processing experiments were con-

ducted using Ti:sapphire laser pulses (800 nm, 1 kHz) in an atmospheric environment. The obtained structure comprises spikes covered with large quantities of nanotubes. Huang et al. [22] fabricated nanoporous anatase TiO₂ on a micro-structured Ti base by using a method involving three steps: femtosecond laser ablation, H₂O₂ oxidation and annealing. In their process, the Ti squares were scanned with a femtosecond laser (1030 nm, 800 fs and 400 kHz) in order to create different microstructures (triangular, square and conical).

All this suggests the simultaneous formation of metal oxides during femtosecond laser processing that substantially benefits photocatalytic properties.

There are a few reports dealing with the photocatalytic properties of laser structured Ti surfaces. Liang et al. have already showed a method for fabricating hierarchical TiO_{2-x} photo electrodes by coupling femtosecond laser processing and anodization [21]. Anodization step caused the covering spikes by TiO₂ nanotubes. This process narrowed the band gap (1.95 eV) and allowed visible light absorption. This hierarchical TiO_{2-x} photoelectrode demonstrated a higher than usual photodegradation rate of MB under visible light ($k_{app} = 53 \times 10^{-3} \text{ min}^{-1}$, which was six times higher than those for P25— $9 \times 10^{-3} \text{ min}^{-1}$). Extended light utilization (up to 636 nm) and synergetic action of spikes and nanotubes may cause excellent results (nanotubes served as a highway during the carriers' transfer). In addition, the MB aqueous solution had a pH = 13.5, so the MB⁺ species are the only ones in the solution. The TiO₂ surface is negatively charged, which increases the adsorption of dye on the catalyst surface. Other studies showing a photocatalytic property of spike-structured Ti have been provided by Huang et al. [22]. They studied degradation of methyl orange. The structured Ti fabricated by femtosecond laser had superior light harvesting properties in the 200–1000 nm wavelength range, which was inherited by annealing TiO₂, resulting in improved photocatalytic degradation of methyl orange under UV-light irradiation compared to nanoporous TiO₂ fabricated by H₂O₂ oxidation and annealing only (without laser fabrication). In this paper, two types of self-organized microstructures were generated using high-power femtosecond laser pulses. The first type of microstructures consists of so-called “herringbone” structures, while the second type consists of typical “spike” structures. The photocatalytic properties of the obtained structures were tested in the methylene blue (model organic pollutant) degradation reaction. The novelty of the presented research is the lack of additional oxidation treatment (no chemical oxidation and annealing) and the use of the as-prepared materials for photocatalysis. Moreover, in the literature cited above, there is no mention of obtaining a herringbone structure on a titanium substrate.

2. Materials and Methods

2.1. Materials

In the present work, a commercially available titanium plate (0.6 mm thick) was cut into smaller pieces of 10 mm × 10 mm and cleaned with ethanol before laser treatment. Subsequently, these smaller plates were mechanically polished to mirror quality surfaces. All reagents were of analytical grade (Merck, Darmstadt, Germany) and were used as received.

2.2. Laser Surface Treatment

The generation of herringbone and spikes structures were conducted by using a femtosecond laser system “PHAROS” at its base wavelength of 1030 nm and with a pulse duration of 266 femtoseconds (Figure 1). The laser exposure was performed in the air. The power and uniformity of the laser beam were monitored by a “Standa” power meter and a high-speed detector, respectively. The spot size was estimated to be 22.67 (1/e² of peak intensity).

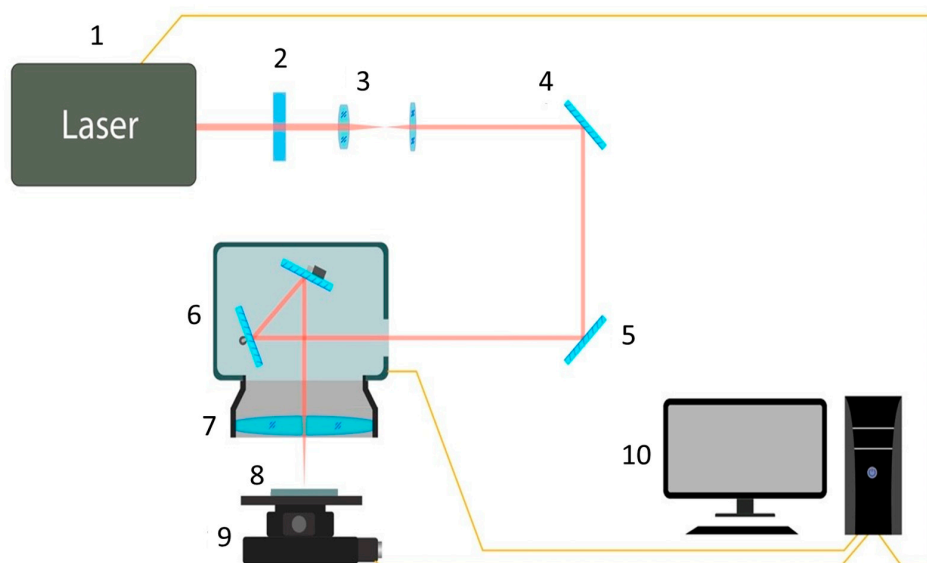


Figure 1. The scheme of the laser setup: laser (1), half-wave plate (2), beam expander (3), mirrors (4, 5), galvanoscanner (6), F-Theta lens (7), sample (8) and six-axis positioner Standa (9), PC (10).

The laser beam trajectory was controlled by the galvanic scanning head according to the preset in the micro-controller. An F-theta lens was used, which allowed processing large area samples without deviating from the focus. The square-shaped samples were processed by a focused laser beam on a 6-axis XYZ motorized table. All laser parameters were summarized in Table 1.

Table 1. Laser parameters used in an experiment.

Sample	Energy per Pulse, E_p (μJ)	Repetition Rate, RR (kHz)	Step (μm)	Scanning Speed, V_s (m/s)	Polarization	Pulse Duration, τ (fs)
P_a	0.9	200	10.5	1.05	\perp	266
P_b	5	1000	9	0.12	\perp	266

2.3. Photocatalytic Experiments

Photocatalytic properties evaluation was performed using methylene blue (MB) as the model compound. The Ti plates (P_a or P_b) were placed in a quartz cuvette, where MB solution was added ($5 \times 10^{-5} \text{ mol dm}^{-3}$, pH = 6). The MB solution without catalyst plate was irradiated parallelly to measuring MB photolysis.

Twelve 9 W lamps (the number of photons per second in a beam ca. 1.84×10^{18}) held at 30 cm from the sample with a 365 nm wavelength were used as the light sources. The catalytic experiment was carried out in six reaction systems summarized in Table 2. The methylene blue decay was monitored spectrophotometrically (UV-Vis 3100 PC spectrophotometer, VWR Ltd., Lutterworth, UK).

Table 2. Photocatalytic reaction systems.

Reaction Systems		H_2O_2 Concentration (%)
Signature	Description	
S1	MB + light	0
S2	MB + P_b + light	0
S3	MB + H_2O_2 + light	1.14
S4	MB + H_2O_2 + P_b + light	1.14
S5	MB + P_a + light	0
S6	MB + H_2O_2 + P_a + light	1.14

3. Results and Discussion

Scanning electron microscope (SEM, Vega3, Tescan, Brno, Czech Republic) operating at 30 kV and equipped with energy-dispersive X-ray detector (EDS, Oxford Instruments, High Wycombe, UK) operating at 15 kV was used to obtain the images of morphology and elemental composition of prepared surfaces. The analysis was carried out over the entire sample area. The elemental composition of samples was assessed by semi-quantitative analysis (resolution of analysis 1%). The chemical composition of the outer layer consists mainly of oxygen and titanium (Table 3).

Table 3. The estimated elemental concentration (atomic percentage) in the outmost layer of Ti plates determined by EDS.

Sample	Ti	O
Ti plate (control)	84	16
P_a	80	20
P_b	46	54

The crystal phases were analyzed using an X-ray diffractometer (XRD; D8 Advance, Bruker, Ettlingen, Germany) with Cu K α ($\lambda = 0.154056$ nm) radiation, operated at 40 kV and 36 mA. Scanning electron microscopy (SEM) images of self-organized nanostructures and microstructures are shown in Figure 2a–f at different magnifications. The titanium plates were treated at 1030 nm wavelength with a focused beam (10 μm at $1/e^2$) scanning the sample surface with two different laser presets, which gave rise to structures named P_a (Figure 2a,c,e) and P_b (Figure 2b,d,f). Laser treatment results in the formation of LIPSS structures on the periphery of the laser spot, while so-called self-organized “spike” structures appear in the central part since the laser beam has a Gaussian shape (Figure 2a,c,e). “Spikes” are self-organized structures that have spherical form in the micrometer scale generated upon polarized ultrashort pulses with energy per pulse well above the ablation threshold. Another condition to form spikes is high repetition rate to maintain the heat accumulation process. Such heat accumulation results in complex hydrodynamic processes, which is also suggested by Tsididis et al. [23]. The period of LIPSS is around 800 nm while the size of a spike is equal to 7–8 microns. Thus, P_a structures can be characterized as heterostructure between nanostructures and microstructures. P_b laser treatment results in the formation of “herringbone” structures (Figure 2b,d,f), which were firstly demonstrated in the work of Garcell et al. [24]. The herringbone structures constitute a singular channel with angled and axially symmetric ripples. Their period is around 10 microns. Comparison of our results and Huang’s [22] results suggests that increasing the repetition rate (>400 kHz) may have resulted in the formation of herringbone structures. The oxide layers were formed on the surface of Ti plates during the laser ablation in the air, and no further oxidative treatment was performed.

The presence of crystalline reflexes in XRD patterns of P_a and P_b samples indicates their crystalline nature (Figure 3B). The observed XRD reflexes can be assigned to Ti (reflexes at 38, 40 and 52.5 $^{\circ}2\theta$) and TiOx (TiO and TiO₂) (36, 38, 41, 42, 53, 61 and 63 $^{\circ}2\theta$) (Figure 3B). No reflections from other phases were observed. The reflexes’ assignment was carried out with the ICDD PDF database [25] and crystallographic open database COD [26]. The Grazing Incidence Diffraction (GID-XRD) allows the study of the surface layer covering the Ti plate. The observed reflexes (36, 42 and 61 $^{\circ}2\theta$) indicate mainly cubic TiO (COD 1536851 and F3m225) in the surface layer (Figure 3A). Different levels of P_a and P_b crystallinity were observed: ~70% (P_a) and ~80% P_b, respectively (measured in the angle range: 20–69 $^{\circ}2\theta$).

EDS measurements showed that the surface of P_b has a higher amount of oxygen atoms than the P_a surface. The SEM images (Figure 1) show differences in the probe’s surface morphology. P_b shows deeper penetration of the titanium plate than the P_a probe; hence, a different composition of the surface layers may be explained.

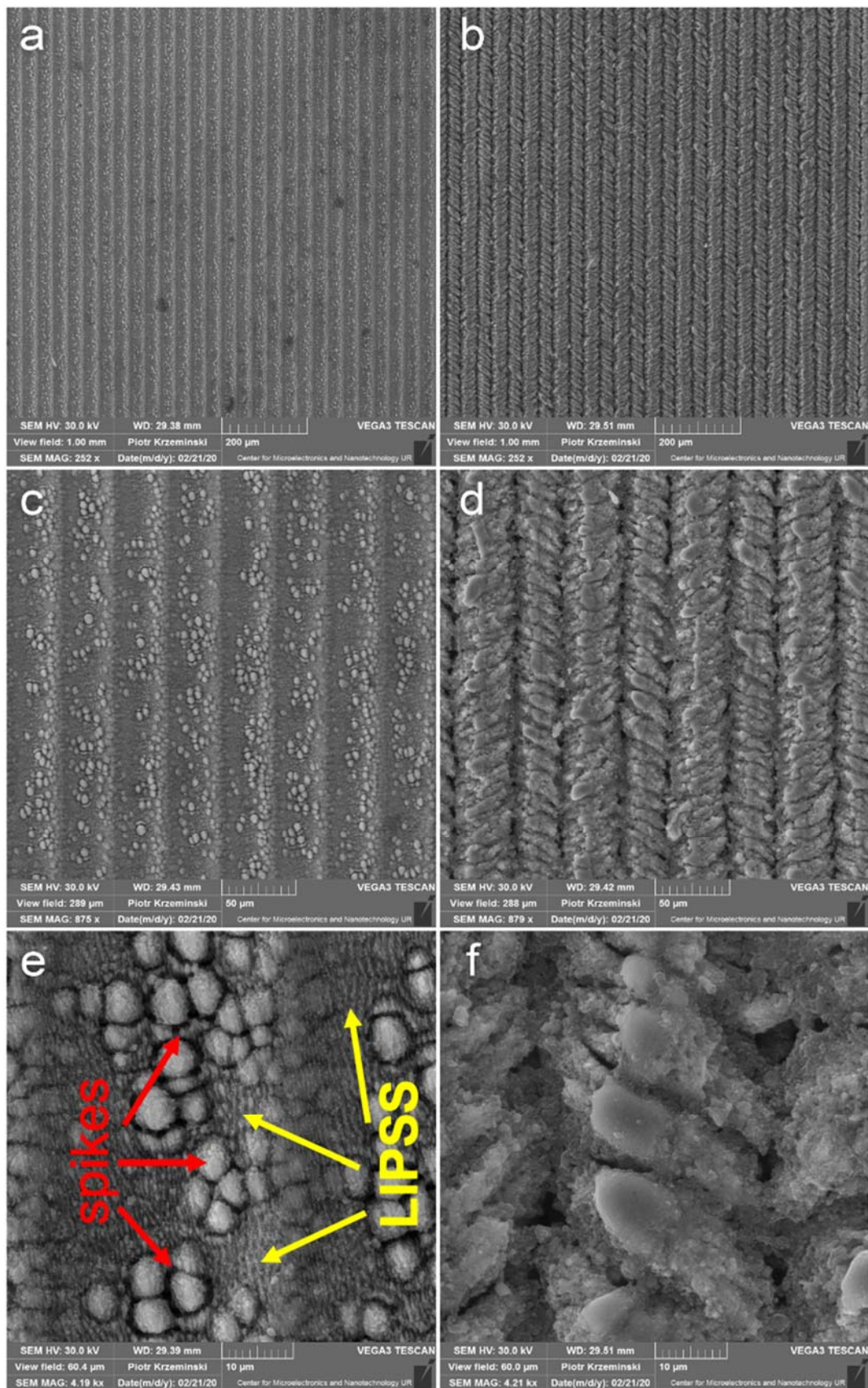


Figure 2. SEM images of surface structured plates (ETD detector with SE mode); “spikes” structures—P_a (a,c,e); and herringbone structures—P_b (b,d,f).

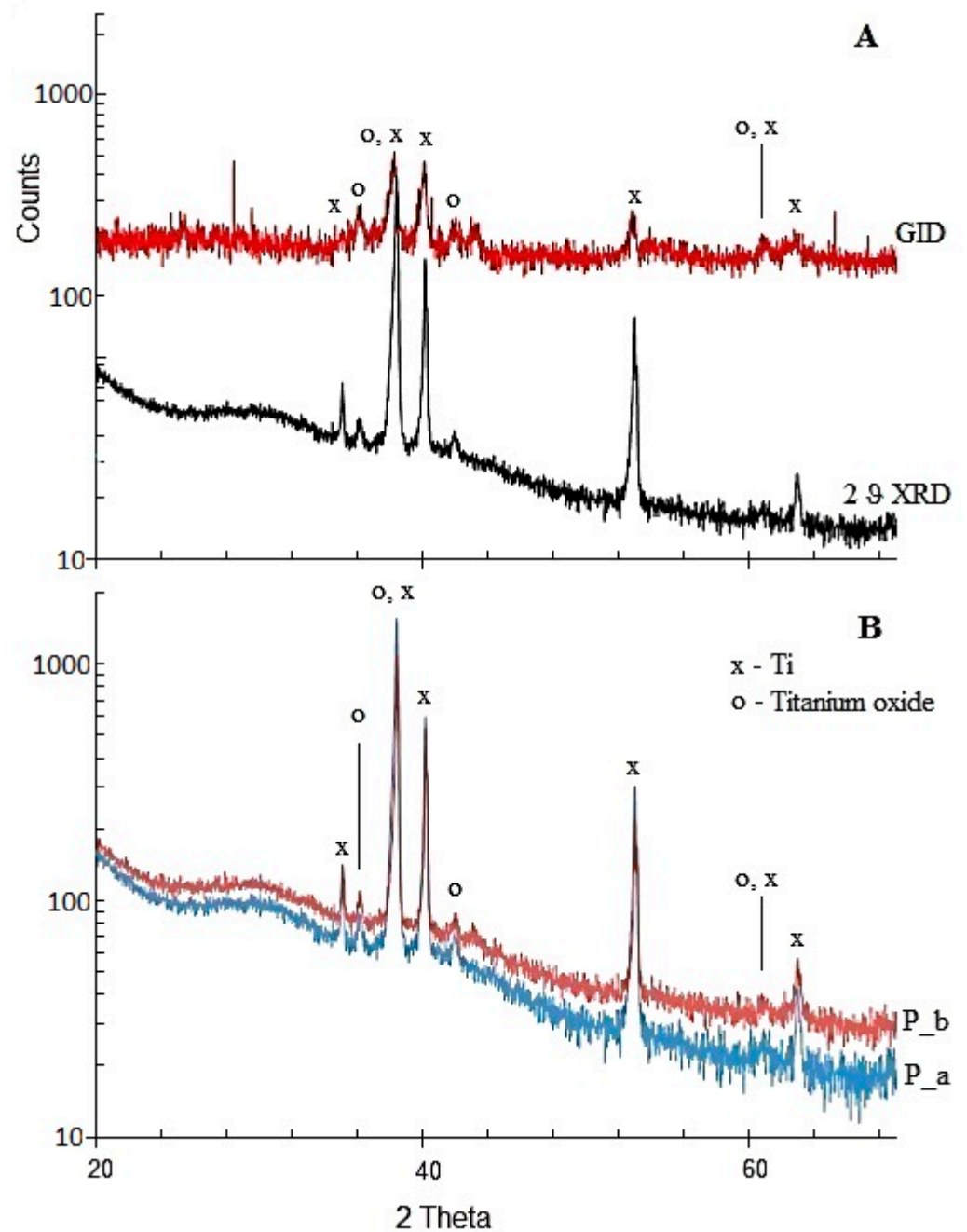


Figure 3. XRD measurements of the following: P_a—sample with “spikes”; P_b—sample with “herringbones”. Comparison of GID and 2θ XRD of P_b sample (A). Crystalline phases analyses in samples: P_a—spikes; P_b—herringbones (B).

Catalytic experiments were carried out in six reaction systems in order to investigate the effect of the presence of the plate’s surface structure on the rate of MB degradation reaction. The photodegradation rate constant (k_{app}) was determined for each degradation system with the assumption that the ongoing reactions were of the first order from Equation (1) [27]:

$$\ln(C/C_0) = -k_{app} t \quad (1)$$

where k_{app} is the apparent rate constant; C_0 and C are the initial concentration and concentration at time t .

A plot of $\ln C_0/C$ versus time represents a straight line, as shown in Figure 4B, where the slope upon linear regression equals the apparent first-order rate constant k_{app} . The obtained degradation rates are summarized in Table 4

Table 4. Kinetic parameters of catalytic reactions.

Reaction System	k_{app} (min^{-1})	$t_{1/2}$ (min)
S1	0.9×10^{-3}	770.1
S2	4.2×10^{-3}	165.0
S3	14.6×10^{-3}	47.8
S4	43×10^{-3}	16.4
S5	27.6×10^{-3}	25.11
S6	6.8×10^{-3}	101.9

MB was photolyzed by direct UV radiation only up to 7.4% in 75 min in the absence of a catalyst (S1, Figure 5). MB irradiation in the presence of P_b caused an increase in MB removal up to 19% (S2 and Figure 5). Comparison of the apparent reaction rate constants (k_{app}) of S1 and S2 show that the degradation of MB in the catalyst's presence (S2) is 4.7 times faster than the photolysis reaction (S1) (Table 3 and Figure 5). Additional H_2O_2 increases the MB degradation efficiency in both systems—without P_b up to 63.5% (S3) and with plate up to 93.5% (S4). The reaction rate of S4 is almost three times that of S3, and it was 47 times that of S1. The degradation efficiency in the presence of P_a is lower in both S5 (33%) and S6 (40.5%) (Figure 5). Miscellaneous MB decay profiles observed for S2 and S5 systems suggest a different reaction route on the surface of the catalysts P_a and P_b.

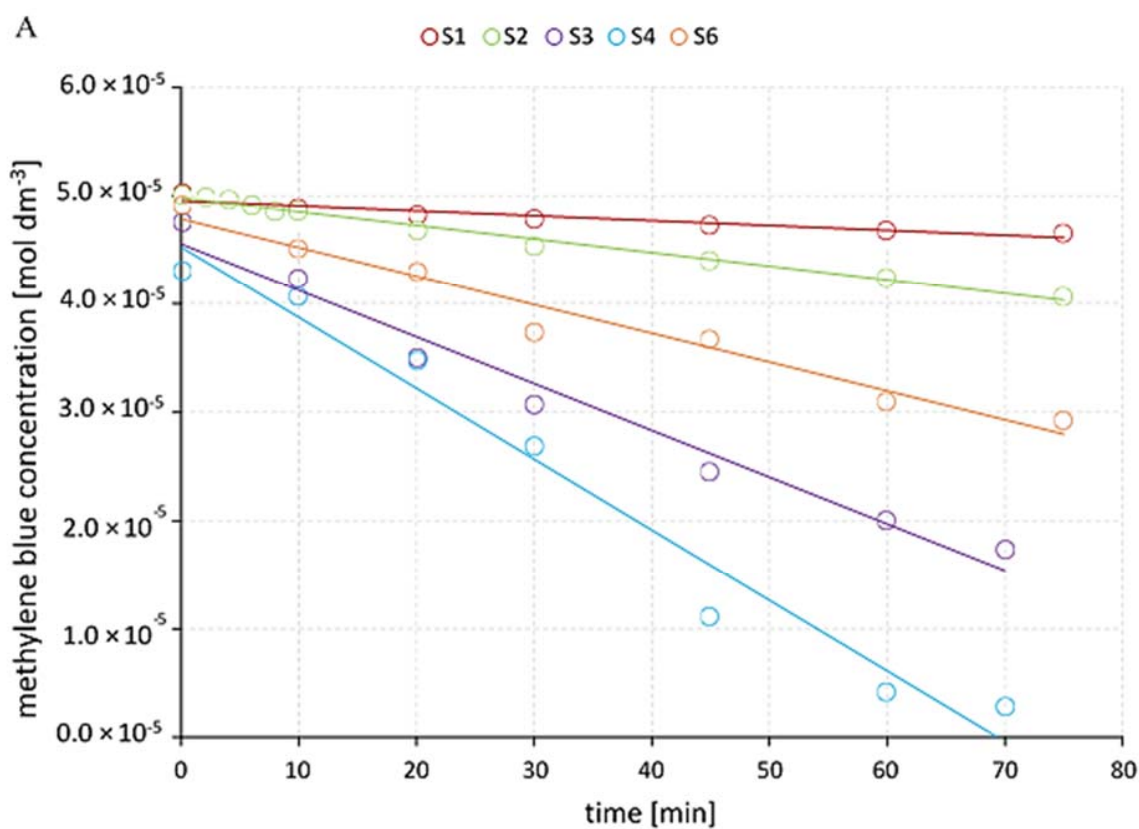


Figure 4. Cont.

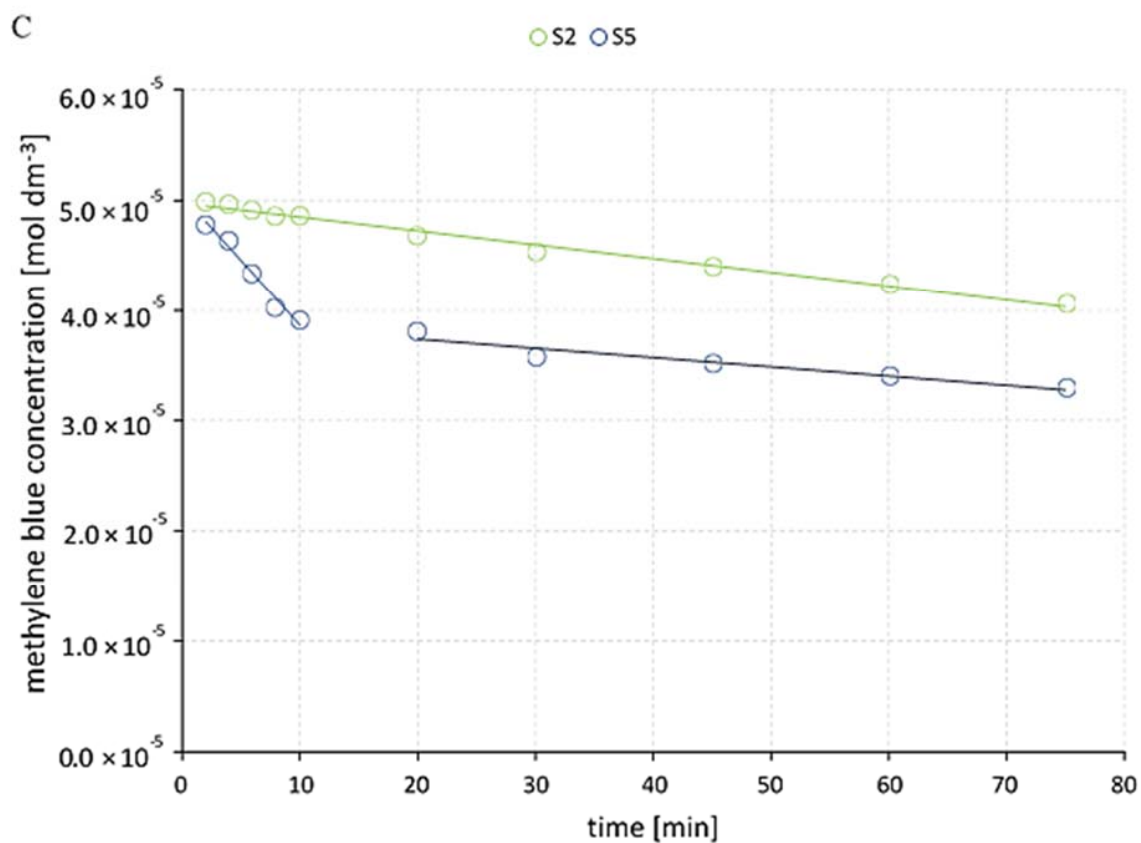
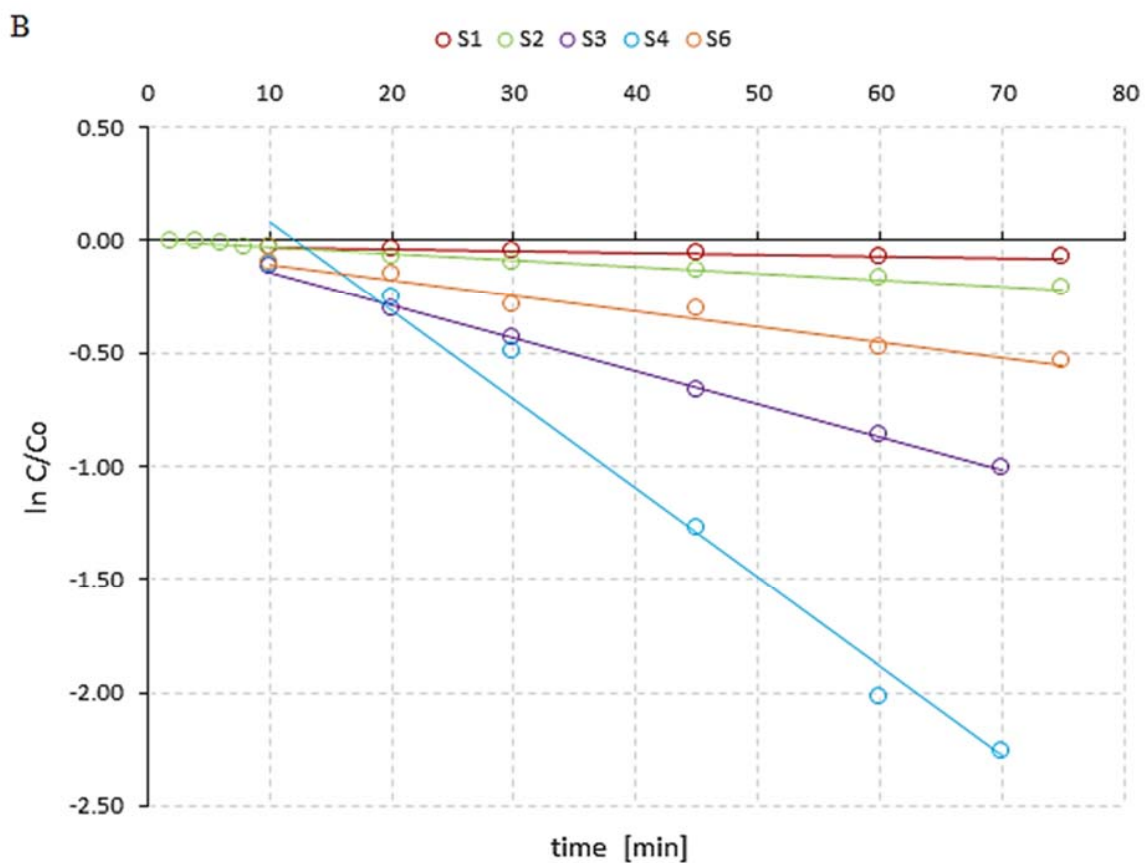


Figure 4. Cont.

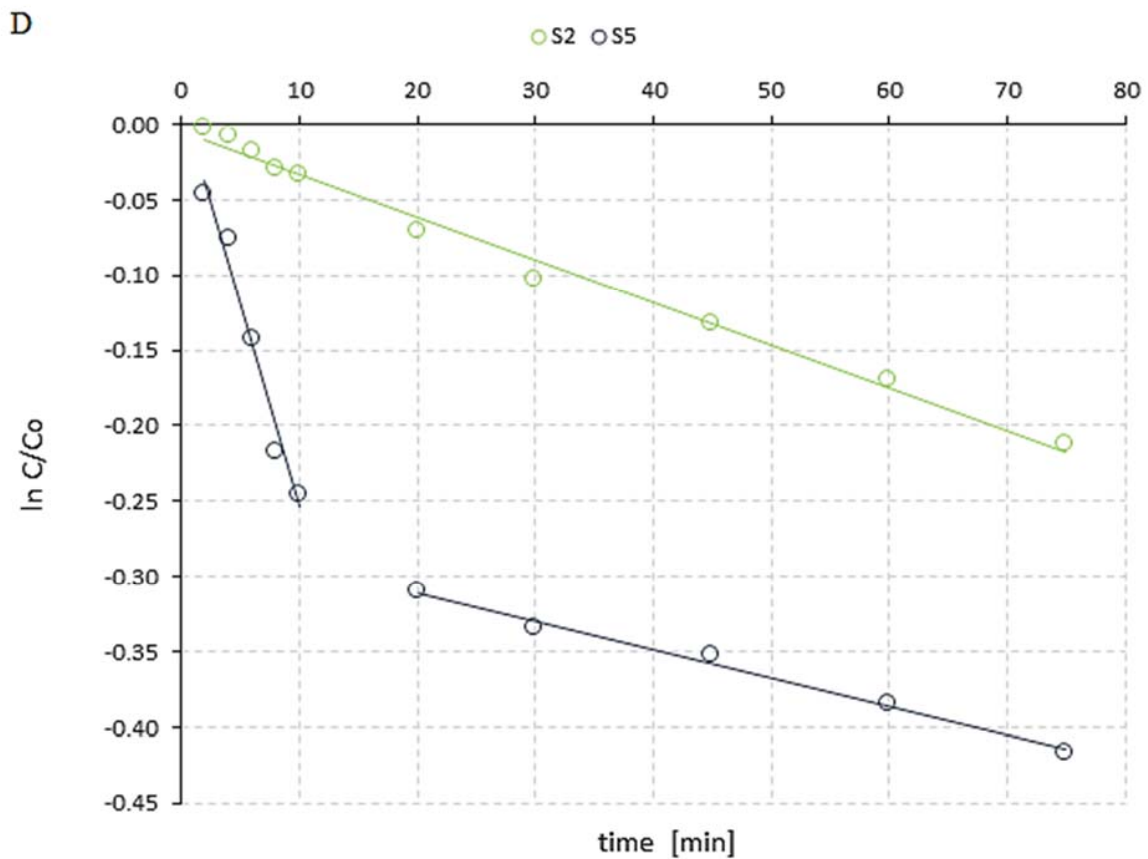


Figure 4. The methylene blue decay rate in all reaction systems (A); degradation kinetics of MB in studied reaction systems (B); MB decay rate on plates (C); MB degradation kinetics on plates (D).

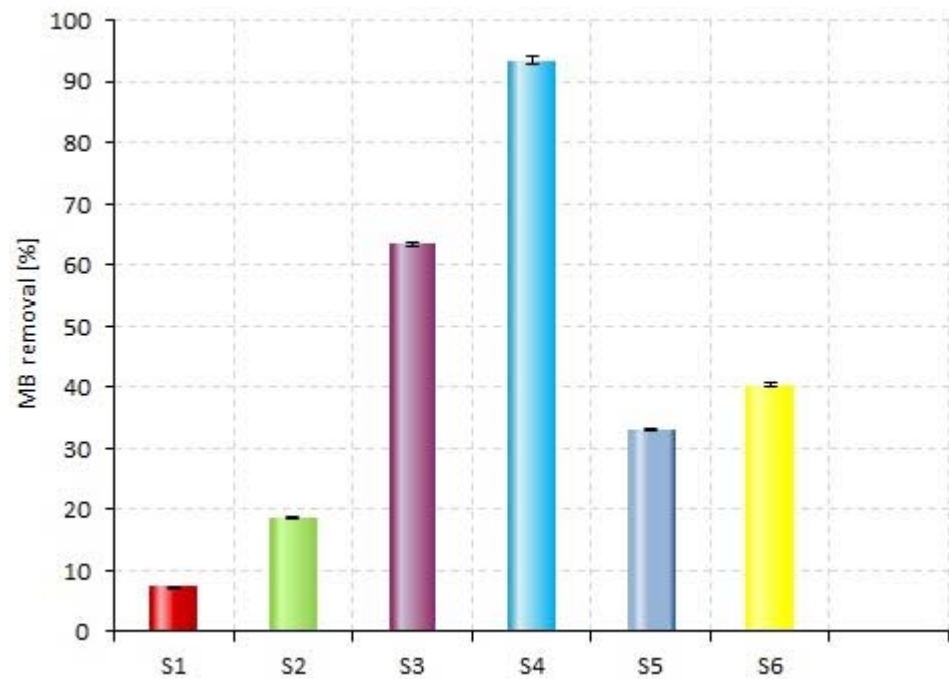


Figure 5. MB removal efficiency in all reaction systems; see Table 2 for description.

The pH of the reaction system may strongly affect the degradation efficiency. The MB can be present in an aqueous solution as the cationic species (MB⁺) and undissociated molecules (MB). The speciation diagram of the MB is shown in Figure 6. As observed

in this figure, the MB species predominates (80%) at pH = 2.7, both MB (50%) and MB+ (50%) species coexist at pH = pKa = 3.14 and MB+ is practically the only species present at pH ≥ 5.5.

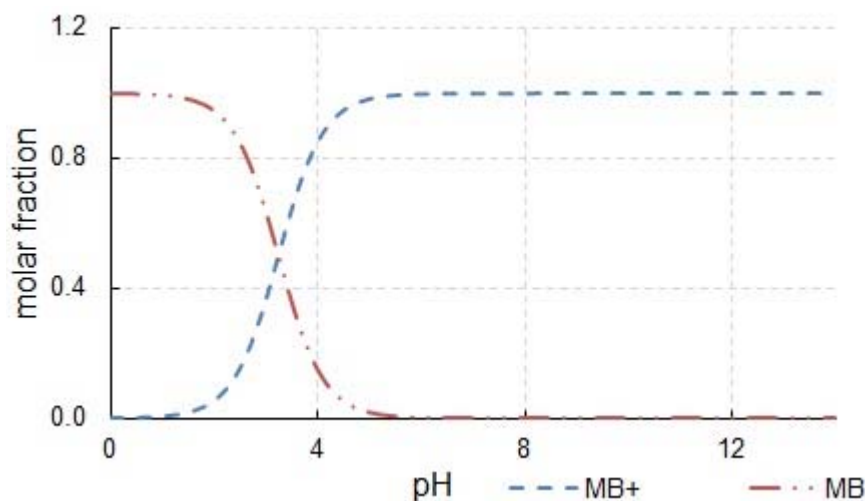


Figure 6. Distribution of MB ionic species depending on the solution pH.

For metal oxide surfaces, the H^+ and OH^- are the charge determining ions [28]. Metal oxides develop a sizable positive surface charge when immersed in water of sufficiently low pH (Equation (2)). Titanium oxide surface at pH = 6 has a positive charge, which may decrease the adsorption of the dye.



The pH may also influence hydroxyl radical generation. There are two possible methods for the generation of hydroxyl radicals in photocatalysis: the first is generation from H_2O_2 by reaction with surface trapped electrons and the second is by reaction of OH^- with surface trapped holes [29]. The catalytic tests were performed with the addition of H_2O_2 as a source of hydroxyl radicals. At very acidic pH values, H_2O_2 is stabilized as $H_3O_2^+$, which is deprotonated and subsequently disproportionates into O_2 and H_2O [30]. In order to avoid the problems mentioned above, pH = 6 was established for photocatalytic tests. This value was obtained after MB dissolved in distilled water (no additional substances were introduced into the reaction system).

A loss of MB at time zero indicates dye adsorption relative to the catalyst surface. In the case of the P_a plate, the loss is 1.96%, while it is 0.425% in the case of the P_b plate. The observed MB+ adsorption suggests that the P_a surface charge is more negative, while the P_b surface is more positive. Hence, the higher efficiency of MB decomposition on the P_a plate. In the case of the reaction S4 and S6, we observed a lower MB degradation efficiency on the P_a plate, which is probably due to the lower production of hydroxyl radicals on the catalyst surface. Adsorbed MB+ reduces the surface availability for H_2O_2 . Hence, the smaller amount of $\bullet OH$ radicals produced.

The results of the EDS analysis showed that the stoichiometry of layer P_a corresponds to the sum formula $TiO_{0.75}$, while the surface P_b has a different stoichiometry with higher oxygen content (probably consists of a mixture of oxides). The cubic compounds TiO_x have a broad homogeneity range with x varying from about 0.75 to 1.30 and the total vacancy content varying between 11 and 20%. The cation and anion vacancy concentrations change continuously over this range in an orderly fashion [31]. In oxygen-deficient TiO_x films, oxygen vacancy energy states are formed below the conduction band minimum [32]. This results in a reduction in the energy required for photoexcitation of electrons and enhancement of the photocatalytic properties. Liang et al. [23] reported high efficiency of MB photodegradation in their work. The estimated k_{app} value was $53 \times 10^{-3} \text{ min}^{-1}$

(pH = 13.5), whereas the value obtained by us in system S4 was $43 \times 10^{-3} \text{ min}^{-1}$. This degradation system seems to be as efficient as the one presented by Liang.

The results of the catalytic tests carried out by us and presented in the literature cannot be compared due to the different composition of the surface layers and completely different conditions of the catalytic processes.

4. Conclusions

The surface of Ti plates was modified by using one-step process and ultrafast and relatively inexpensive methods based on using linearly polarized femtosecond laser pulses. By using the laser, the generated structures comprised titanium oxide layers as “spikes” (P_a) and “herringbones” (P_b). A thorough photocatalytic characterization was performed by using methylene blue (MB) as a model pollutant. The photocatalytic degradation of MB follows the pseudo-first-order reaction kinetics. The MB adsorption on structured surfaces was estimated as losing MB at time zero (before irradiation starting) (MB adsorbed better on P_a than P_b). The results show that the best efficiency of MB degradation was on P_a (systems without H₂O₂, S2 and S5), whereas in systems with H₂O₂ (S4, S6) it was on P_b. This consequence indicates the MB degradation in S2 and S5 systems takes place on the P_a surface, while it takes place in the bulk of solution as a result of reaction with •OH radicals in the S4 and S6 systems. The efficiency of MB removal also confirmed this in the S3 system (MB photolysis in the presence of H₂O₂).

The immobilization of the catalyst on a solid support can be performed in a fast and reproducible manner by using the technique of laser ablation. The layers obtained in this manner have been shown to have catalytic properties. Using other post-structuring processes results in a different composition of the surface layer on the titanium plate.

Author Contributions: J.K. and I.G. contributed to the investigation, formal analysis and writing—original draft preparation; J.K. conducted the catalytic tests; I.G. performed laser surface treatment; B.C. contributed to XRD measurements and analysis; P.K. and M.M. contributed to SEM measurements and analysis; A.B. contributed to data interpretation and discussions; Y.B. supervised the study and writing—review and editing. All authors have read and agreed to the published version of the manuscript.

Funding: The paper was supported by the National Research Fund of Ukraine project 2020.02/0390.

Institutional Review Board Statement: Not applicable.

Informed Consent Statement: Not applicable.

Data Availability Statement: Data available on request due to restrictions e.g., privacy or ethical. The data presented in this study are available on request from the corresponding author. The data are not publicly available. The data are not publicly available because they are part of the ongoing project.

Conflicts of Interest: The authors declare no conflict of interest.

References

1. United States Environmental Protection Agency. *Emerging Technologies for Wastewater Treatment and In-Plant Wet Weather Management*; Report EPA 832-R-12-011; Tetra Tech, Inc.: Fairfax, VA, USA, 2013. Available online: <http://water.epa.gov/scitech/wastetech/publications.cfm> (accessed on 5 September 2021).
2. Stefan, M.I. *Advanced Oxidation Processes for Water Treatment: Fundamentals and Applications*; IWA Publishing: London, UK, 2018.
3. Žerjav, G.; Zavašnik, J.; Kovač, J.; Pintar, A. The influence of Schottky barrier height onto visible-light triggered photocatalytic activity of TiO₂ + Au composites. *Appl. Surf. Sci.* **2021**, *543*, 148799. [[CrossRef](#)]
4. Romoli, L.; Rashed, C.; Fiaschi, M. Experimental characterization of the inner surface in micro-drilling of spray holes: A comparison between ultrashort pulsed laser and EDM. *Opt. Laser Technol.* **2014**, *56*, 35–42. [[CrossRef](#)]
5. Pham, K.X.; Tanabe, R.; Ito, Y. Laser-induced periodic surface structures formed on the sidewalls of microholes trepanned by a femtosecond laser. *Appl. Phys. A* **2012**, *112*, 485–493. [[CrossRef](#)]
6. Gnilitzky, I.; Orazi, L.; Derrien, T.J.-Y.; Bulgakova, N.M.; Mocek, T. Method of Ultrafast Laser Writing of Highly-Regular Periodic Structures on Metallic Materials. Patent of Czech Republic No. PV 2016-424, 27 June 2018.
7. Bonse, J.; Höhm, S.; Hartelt, M.; Spaltmann, D.; Pentzien, S.; Koter, R.; Marschner, S.; Rosenfeld, A.; Krüger, J. *Optically Induced Nanostructures: Biomedical and Technical Applications*; De Gruyter: Berlin, Germany, 2015; pp. 141–156.

8. Gnilitzkiy, I.; Rota, A.; Gualtieri, E.; Valeri, S.; Orazi, L. Tribological Properties of High-Speed Uniform Femtosecond Laser Patterning on Stainless Steel. *Lubricants* **2019**, *7*, 83. [CrossRef]
9. Cunha, A.; Serro, A.; Oliveira, V.; Almeida, A.; Vilar, R.; Durrieu, M.-C. Wetting behaviour of femtosecond laser textured Ti-6Al-4V surfaces. *Appl. Surf. Sci.* **2013**, *265*, 688–696. [CrossRef]
10. Bizi-Bandoki, P.; Benayoun, S.; Valette, S.; Beaugiraud, B.; Audouard, E. Modifications of roughness and wettability properties of metals induced by femtosecond laser treatment. *Appl. Surf. Sci.* **2011**, *257*, 5213–5218. [CrossRef]
11. Wu, B.; Zhou, M.; Li, J.; Ye, X.; Li, G.; Cai, L. Superhydrophobic surfaces fabricated by microstructuring of stainless steel using a femtosecond laser. *Appl. Surf. Sci.* **2009**, *256*, 61–66. [CrossRef]
12. Rotella, G.; Orazi, L.; Alfano, M.; Candamano, S.; Gnilitzkiy, I. Innovative high-speed femtosecond laser nano-patterning for improved adhesive bonding of Ti6Al4V titanium alloy. *CIRP J. Manuf. Sci. Technol.* **2017**, *18*, 101–106. [CrossRef]
13. Fadeeva, E.; Schlie, S.; Koch, J.; Ngezahayo, A.; Chichkov, B.N. The hydrophobic properties of femtosecond laser fabricated spike structures and their effects on cell proliferation. *Phys. Status Solidi* **2009**, *206*, 1348–1351. [CrossRef]
14. Nuutinen, T.; Silvennoinen, M.; Päiväsaari, K.; Vahimaa, P. Control of cultured human cells with femtosecond laser ablated patterns on steel and plastic surfaces. *Biomed. Microdevices* **2013**, *15*, 279–288. [CrossRef]
15. Martínez-Calderon, M.; Silván, M.M.; Rodriguez, A.; Gomez-Aranzadi, M.; García-Ruiz, J.P.; Olaizola, S.M.; Martin-Palma, R.J. Surface micro- and nano-texturing of stainless steel by femtosecond laser for the control of cell migration. *Sci. Rep.* **2016**, *6*, 36296. [CrossRef]
16. Sipe, J.E.; Young, J.F.; Preston, J.; Van Driel, H.M. Laser-induced periodic surface structure. I. Theory. *Phys. Rev. B* **1983**, *27*, 1141–1154. [CrossRef]
17. Shugaev, M.V.; Gnilitzkiy, I.; Bulgakova, N.M.; Zhigilei, L.V. Mechanism of single-pulse ablative generation of laser-induced periodic surface structures. *Phys. Rev. B* **2017**, *96*, 205429. [CrossRef]
18. Shih, C.-Y.; Gnilitzkiy, I.; Shugaev, M.V.; Skoulas, E.; Stratakis, E.; Zhigilei, L.V. Effect of a liquid environment on single-pulse generation of laser induced periodic surface structures and nanoparticles. *Nanoscale* **2020**, *12*, 7674–7687. [CrossRef] [PubMed]
19. Tsukamoto, M.; Kayahara, T.; Nakano, H.; Hashida, M.; Katto, M.; Fujita, M.; Tanaka, M.; Abe, N. Microstructures formation on titanium plate by femtosecond laser ablation. *J. Phys. Conf. Ser.* **2007**, *59*, 666–669. [CrossRef]
20. Heitz, J.; Plamadéala, C.; Muck, M.; Armbruster, O.; Baumgartner, W.; Weth, A.; Steinwender, C.; Blessberger, H.; Kellermaier, J.; Kirner, S.V.; et al. Femtosecond laser-induced microstructures on Ti substrates for reduced cell adhesion. *Appl. Phys. A* **2017**, *123*, 734. [CrossRef]
21. Liang, M.; Li, X.; Jiang, L.; Ran, P.; Wang, H.; Chen, X.; Xu, C.; Tian, M.; Wang, S.; Zhang, J.; et al. Femtosecond laser mediated fabrication of micro/nanostructured TiO₂- photoelectrodes: Hierarchical nanotubes array with oxygen vacancies and their photocatalysis properties. *Appl. Catal. B Environ.* **2020**, *277*, 119231. [CrossRef]
22. Huang, T.; Lu, J.; Zhang, X.; Xiao, R.; Yang, W.; Wu, Q. Femtosecond Laser Fabrication of Anatase TiO₂ Micro-nanostructures with Chemical Oxidation and Annealing. *Sci. Rep.* **2017**, *7*, 2089. [CrossRef] [PubMed]
23. Tsibidis, G.D.; Fotakis, C.; Stratakis, E. From ripples to spikes: A hydrodynamical mechanism to interpret femtosecond laser-induced self-assembled structures. *Phys. Rev. B* **2015**, *92*, 041405. [CrossRef]
24. Garcell, E.M.; Lam, B.; Guo, C. Femtosecond laser-induced herringbone patterns. *Appl. Phys. A* **2018**, *124*, 405. [CrossRef]
25. Kabekkodu, S. *PDF-4+ 2015 (Database)*; International Centre for Diffraction Data: Newtown Square, PA, USA, 2015.
26. Crystallography Open Database. Available online: <http://www.crystallography.net/cod/> (accessed on 5 September 2021).
27. Atkins, P.; De Paula, J. *Atkins' Physical Chemistry*, 8th ed.; W. H. Freeman and Company: New York, NY, USA, 2006; Chapter 22.
28. Tombacz, E. pH-dependent surface charging of metal oxides. *Period. Polytech. Chem. Eng.* **2009**, *53*, 77–86. [CrossRef]
29. Lawless, D.; Serpone, N.; Meisel, D. Role of hydroxyl radicals and trapped holes in photocatalysis. A pulse radiolysis study. *J. Phys. Chem.* **1991**, *95*, 5166–5170. [CrossRef]
30. Babuponnusami, A.; Muthukumar, K. A review on Fenton and improvements to the Fenton process for wastewater treatment. *J. Environ. Chem. Eng.* **2014**, *2*, 557–572. [CrossRef]
31. Banus, M.D.; Reed, T.B.; Strauss, A.J. Electrical and Magnetic Properties of TiO and VO. *Phys. Rev. B* **1972**, *5*, 2775–2784. [CrossRef]
32. Dhumal, S.Y.; Daulton, T.L.; Jiang, J.; Khomami, B.; Biswas, P. Synthesis of visible light-active nanostructured TiO_x (x < 2) photocatalysts in a flame aerosol reactor. *Appl. Catal. B Environ.* **2009**, *86*, 145–151.